Repeating fast radio bursts caused by small bodies orbiting a pulsar or a magnetar

Fabrice Mottez, Guillaume Voisin, Philippe Zarka

Astronomy & Astrophysics manuscript no. 2018˙FRB˙small˙bodies˙pour˙AA˙sub˙cyclotron˙FM˙GV˙PZ˙FM© ESO 2020
February 25, 2020

Repeating fast radio bursts caused by small bodies orbiting a pulsar or a magnetar

Fabrice Mottez[1], Philippe Zarka[2] , Guillaume Voisin[3,1]

[1] LUTH, Observatoire de Paris, PSL Research University, CNRS, Université de Paris, 5 place Jules Janssen, 92190 Meudon, France

[2] LESIA, Observatoire de Paris, PSL Research University, CNRS, Université de Paris, Paris sorbonne Université, 5 place Jules Janssen, 92190 Meudon, France.

[3] Jodrell Bank Centre for Astrophysics, Department of Physics and Astronomy, The University of Manchester, Manchester M19 9PL, UK

February 25, 2020

ABSTRACT

Context. Asteroids orbiting into the highly magnetized and highly relativistic wind of a pulsar offer a favourable configuration for repeating fast radio bursts (FRB). The body in direct contact with the wind develops a trail formed of a stationary Alfvén wave, called an *Alfvén wing*. When an element of wind crosses the Alfvén wing, it sees a rotation of the ambient magnetic field that can cause radio-wave instabilities. In our reference frame, the waves are collimated in a very narrow range of directions, and they have an extremely high intensity.

Aims. A previous work, published in 2014, showed that planets orbiting a pulsar can cause FRB when they pass in our line of sight. We predicted periodic FRB. Since then random FRB repeaters have been discovered. We present an upgrade of this theory to see if they could be explained by the interaction of smaller bodies with a pulsar wind.

Methods. Considering the properties of relativistic Alfvén wings attached to a body in the pulsar wind, and taking thermal consideration into account (the body must be in solid state) we conduct a parametric study.

Results. We find that FRBs can be explained by small size pulsar companions (1 to 10 km) between 0.03 and 1 AU from a pulsar. The intense Lorimer burst (30 Jy) can be explained. Some sets of parameters are also compatible with a magnetar, as suggested for FRB121102. Actually, small bodies orbiting a magnetar could produce (not yet observed) FRBs with $\sim 10^5$ Jy flux density.

Conclusions. This model, after the present upgrade, is compatible with the properties discovered since its first publication in 2014, when repeating FRB were still unknown. It is based on standard physics, and on common astrophysical objects that can be found in any kind of galaxy. It requires 10^{10} times less power than (common) isotropic-emission FRB models.

Key words. FRB, Fast radio burst, pulsar, pulsar wind, pulsar companion, asteroids, Alfvén wing, FRB repeaters, Lorimer burst

1. Introduction

Mottez & Zarka (2014) (hereafter MZ14) proposed a model of FRBs that involves common celestial bodies, neutron stars (NS) and planets orbiting them, well proven laws of physics (electromagnetism), and a moderate energy demand that allows for a narrowly beamed continuous radio-emission from the source that sporadically illuminates the observer. Putting together these ingredients, the model is compatible with the localization of FRB sources at cosmological distances (Chatterjee et al. 2017), it can explain the milliseconds burst duration, the flux densities above 1 Jy, and the range of observed frequencies. The present paper is an upgrade of this model, in the light of the discovery of repeating radio bursts made since the date of publication of MZ14 (Spitler et al. 2016; CHIME/FRB Collaboration et al. 2019). The main purpose of this upgrade is the modeling of the random repeating bursts, and the strong linear polarization possibly associated with huge magnetic rotation measures (Michilli et al. 2018; Gajjar et al. 2018).

The MZ14 model consists of a planet orbiting a pulsar and embedded in its ultra-relativistic wind. From the light-cylinder up to an unknown distance, the wind is highly magnetized. Therefore, in spite of its velocity that is almost the speed of light c, the wind is slower than Alfvèn and fast magnetosonic waves (that are even closer to c). We suppose that the companion is inside this sub-Alfvénic region of the wind. In that case, the body is not shielded behind a shock-wave, but directly in contact with the wind. Then, the disturbed plasma flow reacts by creating a strong potential difference across the companion. This is the source of an electromagnetic wake called Alfven wings because it is formed of one or two stationary Alfven waves. Each AW supports an electric current and an associated change of magnetic field direction. According to MZ14, when the wind crosses an Alfvén wing, it sees a temporary rotation of the magnetic field. This perturbation can be the cause of a plasma instability causing coherent radio waves. Since the pulsar companion and the pulsar wind are permanent structures, this radio-emission process is most probably permanent as well. The source of these radio waves being the pulsar wind when it crosses the Alfvén wings, and the wind being highly relativistic with Lorentz factors up to an expected value $\gamma \sim 10^6$, the radio source has a highly relativistic motion relatively to the radio-astronomers who observe it. Because of the relativistic aberration that results, all the energy in the radio waves is concentrated into a narrow beam of aperture angle $\sim 1/\gamma$ rad (green cone attached to a source S in Fig. 1). Of course, we observe the waves only when we cross the beam. The motion of the beam (its change of direction) results from the orbital motion of the pulsar companion.

Send offprint requests to: e-mail: `fabrice.mottez@obspm.fr`

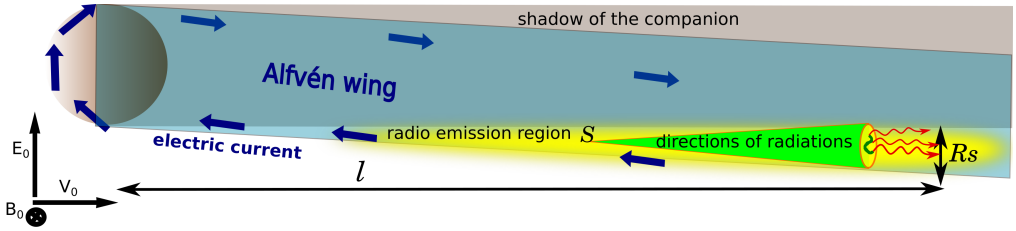

Fig. 1. Schematic view of the area behind a pulsar companion. The pulsar is far to the left-hand side. The wind velocity $\boldsymbol{v}_0$, the wind magnetic field $\boldsymbol{B}_0$ and the convection electric field $\boldsymbol{E}_0$ directions are plotted on the left-hand side. The shadow is in gray. The Alfvén wing is in blue. The region from where we expect radio emissions (in yellow) is inside the wing and outside the shadow. Any point source S in the source region can generate radio waves. Because of the relativistic aberration, their directions are contained in a narrow beam (in green). If the emission is not isotropic in the source reference frame, it is emitted in a subset of this cone (green line from which emerging photons are marked with red arrows. The largest transverse size of the emission region is R_S and its distance to the companion is l.)

The radio-wave energy is evaluated in MZ14, as well as its focusing, and it is shown that it is compatible with a brief emission observable (above 1 Jy) at cosmological distances ($\sim$ 1 Gpc) with flux densities larger than 1 Jy.

Let us notice that in the non-relativistic regime, the Alfvén wings of planet/satellite systems and their radio emissions have been well studied, because this is the electromagnetic structure characterizing the interaction of Jupiter and its rotating magnetosphere with its inner satellites Io, Europa and Ganymede (Saur et al. 2004; Hess et al. 2007; Pryor et al. 2011; Louis et al. 2017; Zarka et al. 2018). It is also observed with the Saturn-Enceladus system (Gurnett et al. 2011).

The upgrade presented here is a generalization of MZ14. In MZ14, it was supposed that the radiation mechanism was the cyclotron maser instability (CMI), a relativistic wave instability that is efficient in the above mentioned solar-system Alfvén wings, with emissions at the local electron gyrofrequency and harmonics (Freund et al. 1983). Here, we consider that other instabilities as well can generate coherent radio emission, at frequencies much lower than the gyrofrequency, as is the case in the highly magnetized inner regions of pulsar environments. Removing the constraint that the observed frequencies are above the gyrofrequency allows for FRB radiation sources, i.e. pulsar companions, much closer to the neutron star. Then, it is possible to explore the possibility of sources of FRB such as belts or streams of asteroids at a close distance to the neutron star. Of course, the ability of these small companions to resist evaporation must be questioned. This is why the present paper contains a detailed study of the companions thermal balance.

The model in MZ14 with a single planet leads to the conclusion that FRBs must be periodic, with a period equal to the companion orbital period, provided that propagation

effects do not perturb too much the conditions of observation. The possibility of clusters of asteroids could explain the existence of non-periodic FRB repeaters, as are those already discovered, because gravitational perturbations would prevent the same asteroid from being exactly on the pulsar-observer line at each orbit.

The present paper contains also a more elaborate reflection than in MZ14 concerning the duration of the observed bursts.

The MZ14 model was not the right one for FRBs since it didn't explain the random timing of FRB repeaters, this is why we upgrade it. Nevertheless, we can already notice that it contains a few elements that have been discussed separately in more recent papers. For instance, the energy involved in this model is smaller by orders of magnitudes than that required by quasi-isotropic emission models, because it involves a very narrow beam of radio emission. This concept alone is discussed in Katz (2017) where it is concluded, as in MZ14, that a relativistic motion in the source, or of the source, can explain the narrowness of the radio beam. This point is the key to the observability of a neutron star-companion system at cosmological distances.

Other ingredients of MZ14, not retained in the present paper, can also be found in the subsequent literature. For instance the idea of maser cyclotron instability for FRBs discussed in MZ14 is the main topic of Ghisellini (2017).

2. Pulsar companion in a pulsar wind: key results

2.1. Alfvén wings

Our hypothesis is that the pulsar wind velocity is less than the Alfvén wave velocity V_A. This is true up to some unknown distance from the light cylinder, in a broad range of latitudes, but probably not everywhere.

In these circumstances, a solid body orbiting a pulsar is not behind a magnetosonic shock wave. It is in direct contact with the pulsar wind. The wind velocity relatively to the orbiting companion $\boldsymbol{V}_w$ crossed with the ambient magnetic $\boldsymbol{B}_w$ field is the cause of an induced electric structure associated with an average field $\boldsymbol{E_0} = \boldsymbol{V}_w \times \boldsymbol{B}_w$, called a unipolar inductor (Goldreich & Lynden-Bell 1969a).

The interaction of the unipolar inductor with the conducting plasma generates a stationary Alfvén wave attached to the body, called Alfvén wing (AW) (Neubauer 1980). The theory of Alfvén wings has been revisited in the context of special relativity by Mottez & Heyvaerts (2011b). In a relativistic plasma flow, the current system carried by each AW (blue arrows in fig. 1), "closed at infinity" has an intensity I_A related to the AW power $\dot{E}_A$ by

$$\dot{E}_A = I_A^2 \mu_0 c, \tag{1}$$

where $\mu_0 c = 1/377$ Mho is the vacuum conductivity.

2.2. Alfvén wing radio emission

By extrapolation of known astrophysical systems, it was shown in MZ14 that the Alfvén wing is a source of radio-emissions of power

$$\dot{E}_R = \epsilon \dot{E}_A \tag{2}$$

where ϵ is estimated to 10^{-3}, and possibly up to 10^{-2}. The resulting flux density at distance D from the source is

$$\left(\frac{\bar{S}}{\mathrm{Jy}}\right) = 10^{-27} A_{\mathrm{cone}} \quad \left(\frac{\epsilon}{10^{-3}}\right)\left(\frac{\gamma}{10^5}\right)^2 \left(\frac{\dot{E}_A}{W}\right) \times \left(\frac{\mathrm{Gpc}}{D}\right)^2 \left(\frac{1\ \mathrm{GHz}}{\Delta f}\right). \tag{3}$$

where Δf is the spectral bandwidth of the emission, γ is the pulsar wind Lorentz factor, and γ^2 in this expression is a consequence of the relativistic beaming: the radio emissions are focused into a cone of characteristic angle $\sim \gamma^{-1}$ when $\gamma >> 1$.

The coefficient A_{cone} is an anisotropy factor. Let Ω_A be the solid angle in which the radio-waves are emitted in the source frame. Then, $A_{\mathrm{cone}} = 4\pi/\Omega_A$. If the radiation is isotropic in the source frame, $A_{\mathrm{cone}} = 1$, otherwise, $A_{\mathrm{cone}} > 1$. For instance, with the CMI, $A_{\mathrm{cone}} \sim 100$.

Since the wing is powered by the pulsar wind, the observed flux density of equation (3) can be related to the properties of the pulsar by expressing $\dot{E}_A$ as a function of P_* and B_*, respectively the spin period and surface magnetic field of the neutron star, and the size of the object R_c. Thus, equation (3) becomes,

$$\left(\frac{\bar{S}}{\mathrm{Jy}}\right) = 6.5\times10^{-6} A_{\mathrm{cone}} \left(\frac{\gamma}{10^5}\right)^2 \left(\frac{\epsilon}{10^{-3}}\right) \left(\frac{R_c}{10^7\mathrm{m}}\right)^2 \times \left(\frac{1\mathrm{AU}}{r}\right)^2 \left(\frac{R_*}{10^4\mathrm{m}}\right)^4 \times \left(\frac{B_*}{10^5\mathrm{T}}\right)^2 \left(\frac{10\mathrm{ms}}{P_*}\right)^2 \left(\frac{\mathrm{Gpc}}{D}\right)^2 \left(\frac{1\ \mathrm{GHz}}{\Delta f}\right). \tag{4}$$

It was proposed in MZ14 that the instability triggering the radio emissions is the cyclotron maser instability (CMI). In spite of its name, the CMI is a fully relativistic phenomenon. We will see that for FRB121102 and other repeaters, the CMI cannot explain the observed frequencies in the context of our model. The plasma process that can generate the observed radio waves is not the topic of the present paper, and, as with coherent radio waves from pulsars, we expect that they depend on a series of plasma characteristics still difficult to constrain. One possibility is that bunched streams of charged particles coherently radiate synchro-curvature radiation as they encounter the magnetic twist of the Alfvén wings, perhaps in a process akin to what has been proposed for the radio emission of the pulsar itself (see Melrose & Rafat (2017) for a recent discussion)

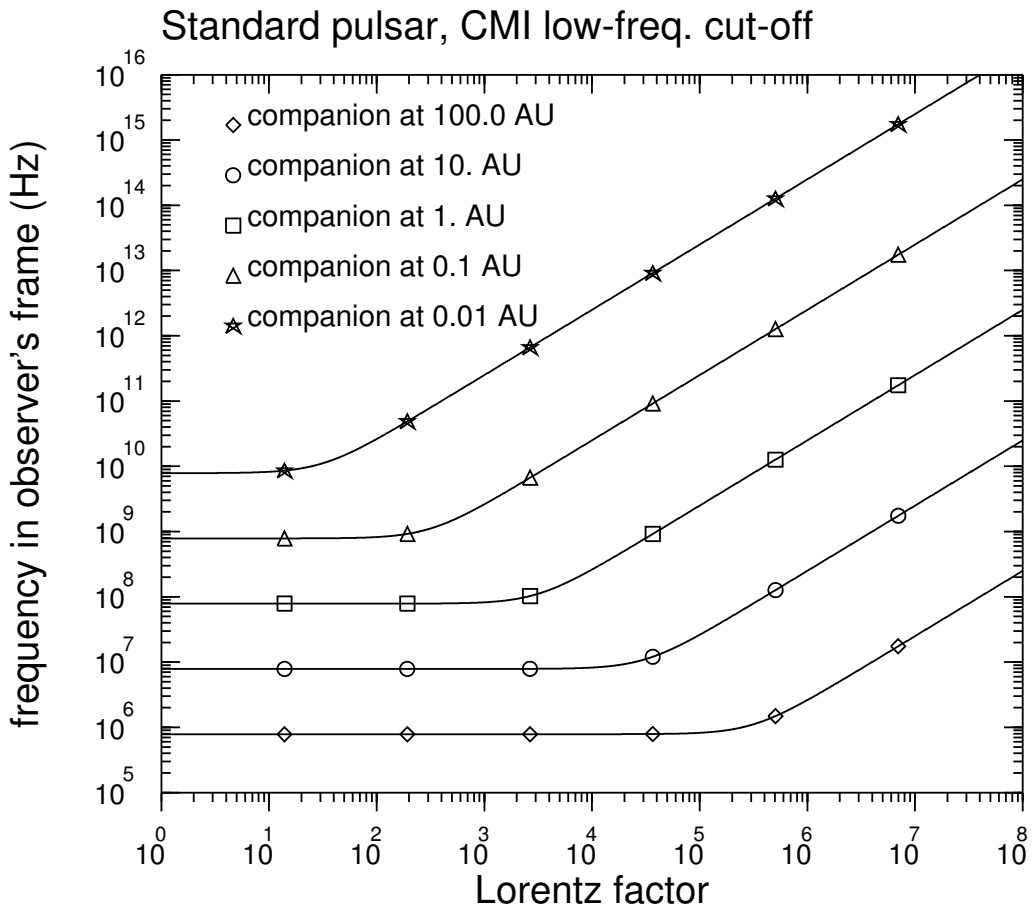

Fig. 2. Electron cyclotron frequency in the observer's frame as a function of the pulsar wind Lorentz factor γ, from Eq. (5) for various distances of the companion. Values that are not varied are the same as in the text and are typical of a standar pulsar: the magnetic field is $B_* = 10^8$ T and the spin period $T_* = 1$ s. This frequency would be the low-frequency cut-off CMI waves.

In any case, we can still use the electron gyrofrequency $f_{ce,o}$ in the observer's frame as a useful scale, From MZ14,

$$\left(\frac{f_{ce,o}}{\mathrm{Hz}}\right) = 2.5\ 10^6 \left(\frac{\gamma}{10^5}\right)\left(\frac{B_*}{10^5\mathrm{T}}\right) \times \left(\frac{1\mathrm{AU}}{r}\right)^2 \left(\frac{R_*}{10^4\mathrm{m}}\right)^2 \times \left\{1 + \left[\frac{\pi\ 10^5}{\gamma}\left(\frac{10\mathrm{ms}}{P_*}\right)\left(\frac{r}{1\mathrm{AU}}\right)\right]^2\right\}^{1/2}. \quad (5)$$

When it is much larger than the observed radio frequencies of FRBs, the CMI can be discarded.

Figure 2 shows the dependence of the frequency on the wind Lorentz factor γ for various distances r between the NS and its companion. This is computed for a standard pulsar, with $P_* = 1$ s and $B_* = 10^8$ T.

3. Asteroid heating

3.1. Overview

The asteroid is heated by several distinct sources (see Table 1). Their effect can be quantified with the heating power $\dot{E}$ measured in W.

The first two categories of thermal energy for the companion are the thermal radiation of the neutron star, of luminosity L_T, and the energy resulting from the loss of rotational energy of the neutron star $\dot{E}_{rp}$. This last contribution is transformed inside the pulsar inner magnetosphere into a Poynting flux, into the sum of a pulsar wave Poynting flux, into the pulsar wind kinetic energy, and into non-thermal high energy radiation.

Heating by the black-body radiation of the neutron star is a particular case of a basic phenomenon experimented by any kind of body orbiting any kind of star. The associated flux is noted $\dot{E}_T$ (T for thermal). But the photon luminosity of the pulsar is not entirely composed of its thermal radiation, because of the gamma rays and of the X rays emitted by the accelerated particles in the magnetosphere. We can note $\dot{E}_{NT}$ the contribution of the non-thermal photons.

Heating by the Poynting flux carried by the pulsar wave is more specific. This wave is associated with the fast rotation of the neutron star magnetic field at the frequency Ω_*. It has a velocity c. It is a source of inductive heating. The associated heating power $\dot{E}_P$ can be computed locally (nearby the companion) as the effect of a plane wave on a spherical conducting body.

The companion is also heated by direct absorption of the energy carried by the particles ejected by the pulsar (that is the pulsar wind beyond the light cylinder). We note $\dot{E}_W$ the heating power of the particles in the pulsar wind.

Another process must be taken into account if the companion is immersed in a sub-Alfvénic wind : Joule heating by the Alfvén wing, associated with a power $\dot{E}_J$.

Let us investigate these sources of heat for the companion. We compute the corresponding $\dot{E}_T, \dot{E}_{NT}, \dot{E}_P, \dot{E}_W, \dot{E}_J$ for each of these sources. Then, the thermal equilibrium temperature T_c of the pulsar companion is

$$\dot{E}_T + \dot{E}_{NT} + \dot{E}_P + \dot{E}_W + \dot{E}_J = 4\pi\sigma_S R_c^2 T_c^4, \tag{6}$$

where σ_S is the Stefan-Boltzmann constant, and R_c and T_c are radius and temperature of the companion object respectively.

3.2. Heating by thermal radiation from the neutron star

For heating by the star thermal radiation,

$$\dot{E}_T = \frac{L_T}{4}\left(\frac{R_c}{r}\right)^2 \text{ and } L_T = 4\pi\sigma_S R_*^2 T_*^4 \tag{7}$$

Table 1. Notations for powers $\dot{E}$ absorbed by the NS companion, and pulsar luminosities L, their origin, and where they are evaluated in the present paper.

Notation	Origin	Which section
$\dot{E}_A$	electromagnetic power of the Alfvén wing	section 2.1
$\dot{E}_T$ L_T	neutron star thermal radiation	section 3.2
$\dot{E}_{NT}$ L_{NT}	pulsar non-thermal photons	section 3.4
$\dot{E}_P$	Poynting flux of pulsar wave	section 3.3
$\dot{E}_W$ L_W	particles in the pulsar wind	section 3.5
$\dot{E}_J$	Joule heating by the Alfvén wing current	section 3.7
$f\dot{E}_{\rm rp}$	fraction of pulsar rotational energy loss injected into the pulsar wave Poynting flux	section 3.3
$(1-f)g\dot{E}_{\rm rp}$	fraction of pulsar rotational energy loss transformed into wind particle energy and non-thermal radiation in the direction of the companion	section 3.6

where L_T is the thermal luminosity of the pulsar, R_* and T_* are the neutron star radius and temperature, σ_S is the Stefan-Boltzmann constant and in international system units, $4\pi\sigma_S = 7.\,10^{-7}$ W.m^{-2}.K^{-4}. For $T_* = 10^6$ K, and $T_* = 0.3 \times 10^6$, the luminosities are respectively $7. \times 10^{25}$ W and 10^{24} W. This is consistent with the thermal radiation of Vela observed with Chandra, $L_T = 8 \times 10^{25}$ W (Zavlin 2009).

3.3. Heating by the pulsar wave Poynting flux

Heating by the Poynting flux has been investigated in Kotera et al. (2016). Following their method,

$$\dot{E}_P = \left(\frac{f\dot{E}_{\rm rp}}{f_p}\right)\left(\frac{Q_{\rm abs}}{4}\right)\left(\frac{R_c}{r}\right)^2 \tag{8}$$

where $\dot{E}_{\rm rp}$ is the loss of pulsar rotational energy (rp is for rotational power).

The product $f\dot{E}_{\rm rp}$ is the part of the rotational energy loss that is taken by the pulsar wave. The dimensionless factor f_p is the fraction of the sky into which the pulsar wind is emitted. The absorption rate $Q_{\rm abs}$ of the Poynting flux by the companion is derived in Kotera et al. (2016) by application of the Mie theory with the Damie code based on Lentz (1976). For a metallic body whose size is less than $10^{-2}R_{LC}$, $Q_{\rm abs} < 10^{-6}$ (see their Fig. 1). We note $Q_{\rm max} = 10^{-6}$ this upper value.

The value $Q_{\rm max} = 10^{-6}$ may seem strangely small. Indeed, for a large planet, we would have $Q \sim 1$. To understand well what happens, we can make a parallel with the propagation of electromagnetic waves in a dusty interstellar cloud. The size of the dust grains is generally ~ 1 μm. Then, visible light, with smaller wavelengths (~ 500 nm) is scattered by these grains. But infrared light, with a wavelength larger that the dust grains is, in accordance with the Mie theory, not scattered, and the dusty cloud is transparent

to infrared light. With a rotating pulsar, the wavelength is the "vacuum wave" (Parker spiral) of wavelength $\lambda \sim 2c/\Omega_*$ equal to twice the light cylinder radius $r_{LC} = c/\omega_*$. Dwarf planets are comparable in size with the light cylinder of a millisecond pulsar and much smaller than a 1s pulsar, therefore smaller bodies always have a factor Q smaller or much smaller than 1. Asteroids up to 100 km are smaller than the light cylinder, therefore they don't scatter, neither absorb, the energy carried by the pulsar "vacuum" wave. This is what is expressed with $Q_{\max} = 10^{-6}$.

3.4. Heating by the pulsar non-thermal radiation

For heating by the star non-thermal radiation,

$$\dot{E}_{NT} = g_{NT} \frac{L_{NT}}{4} \left(\frac{R_c}{r} \right)^2 \tag{9}$$

where g_{NT} is a geometrical factor induced by the anisotropy of non-thermal radiation. In regions above non-thermal radiation sources, $g_{NT} > 1$, but in many other places, $g_{NT} < 1$. The total luminosity associated with non-thermal radiation L_{NT} depends largely on the physics of the magnetosphere, and it is simpler to use measured fluxes than those predicted by models and simulations.

With low-energy gamma-ray-silent pulsars, most of the energy is radiated in X-rays. Typical X-ray luminosities are in the range $L_X \sim 10^{25} - 10^{29}$ W, corresponding to a proportion $\eta_X = 10^{-2} - 10^{-3}$ of the spin-down luminosity $\dot{E}_{\rm rp}$ (Becker 2009).

Gamma-ray pulsars are more energetic. It is reasonable to assume gamma-ray pulsar luminosities $L_\gamma \sim 10^{26} - 10^{29}$ W (Zavlin 2009; Abdo et al. 2013). The maximum of these values can be reached with young millisecond pulsars. For instance, the the Crab pulsar (PSR B0531+21), with a period $P_* = 33$ ms and $B_* = 10^{8.58}$ T has the second largest known spin-down power $\dot{E}_{\rm rp} = 10^{31.66}$ W and its X-ray luminosity is $L_X = 10^{29}$ W (Becker 2009). Its gamma-ray luminosity, estimated with Fermi is $L_\gamma = 6.25 \times 10^{28}$ W above 100 MeV (Abdo et al. 2010b). Vela ($P_* = 89$ ms, $B_* = 10^{8.5}$ T) has a lower luminosity: $L_X = 10^{25.8}$ W in X-rays (including the already mentioned contribution of thermal radiation) and $L_\gamma = 8.2 \times 10^{27}$ W in gamma-rays (Abdo et al. 2010a).

Concerning the geometrical factor g_{NT}, it is important to notice that most of the pulsar X-ray and gamma-ray radiations are pulsed. This means that their emission is not isotropic.Without going into the diversity of models that have been proposed to explain the high-energy emission of pulsars it is clear that i) the high-energy flux impinging on the companion is not constant and should be modulated by a duty cycle and ii) the companion may be located in a region of the magnetosphere where the high-energy flux is very different from what is observed, either weaker or stronger. It would be at least equal to or larger than the inter-pulse level.

If magnetic reconnection takes place in the stripped wind (see Pétri (2016) for a review), presumably in the equatorial region, then a fraction of the Poynting flux L_P

would be converted into high-energy particles, either X-ray and gamma-ray photons (or accelerated leptons, see section 3.5), which would also contribute to the irradiation. At what distance ? Some models based on a low value of the wind Lorentz factor ($\gamma = 250$ in Kirk et al. (2002)) evaluate the distance r_{diss} of the region of conversion as 10 to 100 r_{LC}. With pulsars with $P \sim 0.01$ or 0.1 s as we will see later, the companions would be exposed to a high level of X and gamma-rays. But, as we will see, the simple consideration of γ as low as 250 does not fit our model. More recently, Cerutti & Philippov (2017) showed with numerical simulations a scaling law for $r_{diss}/R_{LC} = \pi\gamma\kappa_{LC}$ where κ_{LC} is the plasma multiplicity at the light cylinder. With multiplicities of order $10^3 - 10^4$ (Timokhin & Arons 2013) and $\gamma > 10^4$ (Wilson & Rees 1978; Ng et al. 2018), and the "worst case" $P_* = 1$ ms, we have $r_{diss} > 3$ AU, that is beyond the expected distance r of the companions causing FRBs, as will be shown in the parametric study (section 7).

Therefore, we can consider that the flux of high energy photons received by the pulsar companions is less than the flux corresponding to an isotropic luminosity L_{NT}, therefore we can consider that $g_{NT} \leq 1$.

3.5. Heating by the pulsar wind particles that hit the companion

Heating by absorption of the particle flux can be estimated on the basis of the density of electron-positron plasma that is sent away by the pulsar with an energy $\sim \gamma m_c c^2$. Let n be the number density of electron-positron pairs, we can write $n = \kappa\rho_G/e$ where ρ_G is the Goldreich-Julian charge density (also called co-rotation charge density), κ is the multiplicity of pair-creations, and e is the charge of the electron. We approximate $\rho_G = 2\epsilon_0\omega_* B_*$. Then,

$$L_W = \kappa n_G \gamma m_e c^2 4\pi R_*^2 f_W \tag{10}$$

where $f_W \leq 1$ is the fraction of the neutron star surface above which the particles are emitted. The flux $\dot{E}_W$ is deduced from L_W in the same way as in Eq. (9),

$$\dot{E}_W = g_W \frac{L_W}{4} \left(\frac{R_c}{r}\right)^2 \tag{11}$$

and g_W is a geometrical factor depending on the wind anisotropy.

3.6. Added powers of the wind particles and of the pulsar non-thermal radiation

We can notice in Eq. (10) that the estimate of L_W depends on the ad-hoc factors κ, γ and f. Their estimates are highly dependent on the various models of pulsar magnetosphere. It is difficult to estimate L_{NT} Then, it convenient to notice that there are essentially two categories of energy fluxes: those that are fully absorbed by the companion (high-energy particles, photons and leptons), and those that may be only partially absorbed (the Poynting flux). Besides, all these fluxes should add up to the total rotational energy loss

of the pulsar $\dot{E}_{\rm rp}$. Therefore, the sum of the high-energy contributions may be rewritten as being simply

$$g_W L_W + g_{NT} L_{NT} = (1-f) g \dot{E}_{\rm rp} \tag{12}$$

where f is the fraction of rotational energy loss into the pulsar wave, already accounted for in Eq. (8). This way of dealing with the problem allows an economy of ad-hoc factors. The dependency of g is a function of the inclination i of the NS magnetic axis relatively to the companion orbital plane is a consequence of the effects discussed in section 3.4. Following the discussion of the previous sections regarding g_W and g_{NT}, we assume generally that g is less than one.

3.7. Heating by the companion Alfvén wing

There is still one source of heat to consider : the Joule dissipation associated with the Alfvén wing electric current. The total power associated with the Alfvén wing is

$$\dot{E}_A \sim I_A^2 \mu_0 V_A = I_A^2 \mu_0 c. \tag{13}$$

where $V_A \sim c$ is the Alfvén velocity, and I_A is the total electric current in the Alfvén wing. A part $\dot{E}_J$ of this power is dissipated into the companion by Joule heating

$$\dot{E}_J = \frac{I_A^2}{\sigma_c h} = \frac{\dot{E}_A}{\mu_0 c \sigma_c h} \tag{14}$$

where σ_c is the conductivity of the material constituting the companion, and h is the thickness of the electric current layer. For a small body, relatively to the pulsar wavelength c/Ω_*, we have $h \sim R_c$. For a rocky companion, $\sigma_c \sim 10^{-3}$ Mho.m^{-1}; and for iron, $\sigma_c \sim 10^7$ Mho.m^{-1}.

Actually, the AW takes its energy from the pulsar wave Poynting flux, and we could consider that $\dot{E}_A$ is also a fraction of the power $f\dot{E}_R$. We could then conceal this term in the estimate of f. Nevertheless, we keep it explicitly for the estimate of the minimal companion size that could trigger a FRB, because we need to know $\dot{E}_A$ for the estimation of the FRB power.

4. The minimal companion size required for FRB

The pulsar companion can survive only if it does not evaporate. As we will see in the parameteric studies, the present model works better with metallic companions. Therefore, we anticipate this result and we consider that its temperature must not exceed the iron fusion temperature $T_{\rm max} \sim 1400$ K. Equation (6) with $T_{\rm max}$ provides an upper value of $\dot{E}_A$, and Eq. (3) with a minimum value $S = 1$ Jy provides a lower limit $\dot{E}_{Amin}$ of $\dot{E}_A$. The combination of these relations sets a constrain on the companion radius

$$R_c^3 \mu_0 c \sigma_c \left[4\pi\sigma_S T_{\rm max}^4 - \frac{X}{4r^2} \right] > \dot{E}_{Amin} \tag{15}$$

where E_{Amin} is given by Eq. (3) with $S = 1$ Jy, and

$$X = 4\pi R_*^2 \sigma_S T_*^4 + ((1-f)g + \frac{f}{f_p} Q_{\rm abs}) \dot{E}_{\rm rp} \tag{16}$$

Because the coefficient of inductive energy absorption $Q_{\rm abs} < Q_{\rm max} = 10^{-6}$, and f_p is a larger fraction of unity than $Q_{\rm abs}$, we can neglect the contribution of inductive heating $\dot{E}_P$. Combined with Eq. (3), with $T_{\rm max} = 1400$ K for iron fusion temperature, and with normalized figures, we finally get the condition for the companion to remain solid:

$$R_c^3 \left(\frac{\sigma_c}{10^7 Mho}\right) \left[2.7\,10^4 \left(\frac{T_c}{1400K}\right)^4 - \left(\frac{AU}{r}\right)^2 X\right] > 2.7\,10^{15} \frac{Y}{A_{\rm cone}} \tag{17}$$

where

$$X = 7 \left(\frac{R_*}{10^4 m}\right)^2 \left(\frac{T_*}{10^6 K}\right)^4 + (1-f)g \left(\frac{\dot{E}_{\rm rp}}{10^{25} W}\right) \tag{18}$$

and

$$Y = \left(\frac{S_{min}}{Jy}\right) \left(\frac{10^5}{\gamma}\right)^2 \left(\frac{10^{-3}}{\epsilon}\right) \left(\frac{D}{Gpc}\right)^2 \left(\frac{\Delta f}{GHz}\right). \tag{19}$$

We note that f, g and $\dot{E}_{\rm rp}$ count for a single free parameter of this model, in the form $(1-f)g\dot{E}_{\rm rp}$ that appears only once, in Eq. (18). We also note that when, for a given distance r, the factor of R_c^3 in Eq. (15) is negative, then no FRB emitting object orbiting the pulsar can remain in solid state, whatever its radius.

5. Clusters and belts of small bodies orbiting a pulsar

With FRB121102, no periodicity was found in the time distribution of bursts arrival. Therefore, we cannot consider that they are caused by a single body orbiting a pulsar. Scholz et al. (2016) have shown that the time distribution of bursts of FRB121102 is clustered. Many radio-surveys lasting more than 1000 s each and totaling 70 hours showed no pulse occurrence, while 6 bursts were found within a 10 min period. The arrival time distribution is clearly highly non-Poissonian. This is somewhat at odds with FRB models based on pulsar giant pulses which tend to be Poissonian (Karuppusamy et al. 2010).

We suggest that the clustered distribution of repeating FRBs could result from a small number of swarms of asteroid. It could also be a small group of planets possibly with satellites (larger than a few hundreds of km).

The hypothesis of clustered asteroids seems to be confirmed by the recent detection of a 16.35 ± 0.18 day periodicity from a repeating FRB 180916.J0158+65 detected by the Canadian Hydrogen Intensity Mapping Experiment Fast Radio Burst Project (CHIME/FRB). In 28 bursts recorded from 16th September 2018 through 30th October 2019,it is found that bursts arrive in a 4.0-day phase window, with some cycles showing no bursts, and some showing multiple bursts (The CHIME/FRB Collaboration et al. 2020).

Other irregular sources could be considered. We know that planetary systems exist around pulsar, if uncommon. One of them has four planets. It could as well be a system formed of a massive planets and Trojan asteroids. In the solar system, Jupiter has about 1.6×10^5 L4 Trojan asteroids bigger than 1 km radius (Jewitt et al. 2000). Some of them reach larger scales: 588 Achilles, discovered in 1906, measures about 135 kilometers in diameter, and 617 Patroclus, 140 km in diameter, is double. The Trojan satellites have a large distribution of eccentric orbits around the Lagrangian points (Jewitt et al. 2004). If they were observed only when they are rigorously aligned with, say, the Sun and Earth, the times of these passage would look quite non-periodic, non-Poissonian, and most probably clustered. The FRB 180804 was observed over 300 hours with WSRT/Aperitif, and no burst was detected. This suggests, among two other possibilities (a very soft radio spectrum, or an extinction of the FRB source (Cordes et al. 2017)), a high degree of clustering of its bursts (Oostrum et al. 2019).

Gillon et al. (2017) have shown that rich planetary systems with short period planets are possible around main sequence stars. There are seven Earth-sized planets in the case of Trappist-1, the farther one having an orbital period of only 20 days. Let us imagine a similar system with planets surrounded by satellites. The times of alignment of satellites along a given direction would also seem quite irregular, non-Poissonian and clustered. One could object that such complicated system are not expected to exist around pulsars. But actually, most of the exo-planetary systems discovered in the last 20 years should have been excluded from the standard models used before their discovery, and the low-eccentricity orbits of the planets orbiting pulsars (Wolszczan & Frail 1992) are in this lot. Also very interesting is the plausible detection of an asteroid belt around PSR B1937+21 (Shannon et al. 2013) which effect is visible only as red timing noise. It is permitted to believe that there exists other pulsars where such belts might be presently undistinguishable from other sources of red noise (see e.g. Shannon et al. (2014) and references therein). So, we think that is it not unreasonable to consider swarms of small bodies orbiting a pulsar, even if they are not yet considered as common according to current representations.

6. Bursts duration

Two characteristics must be discussed regarding the duration of the bursts : the narrowness and the small dispersion of their duration. For the first 17 events associated with FRB121102 in the FRB Catalog (Petroff et al. 2016) [1], the average duration duration is 5.1 ms and the standard deviation is 1.8 ms [2].

[1] http://www.frbcat.org

[2] We can notice that for all FRB found in the catalog, where FRB121102 counts for 1 event, the average width, 5.4 ms, is similar to that of FRB121102, and the standard deviation is 6.3 ms

Considering a circular Keplerian orbit of the NS companion, the time interval τ during which radio waves are seen is the sum of a time τ_1 associated with the angular size of the beam (size of the dark green area inside the green cone in fig. 1), and a time τ_2 associated with the size of the source (size of the yellow region in fig. 1). The two are convoluted with the orbital velocity of the NS companion. In MZ14, the term τ_2 was omitted, here is a correction to this error.

The time τ_1 to cross the cone was estimated in MZ14 for various values of the wind Lorentz factor γ. For an isotropic emission in the source frame, this time was estimated to 1.3 s with $\gamma = 10^5$ and 0.13 s with $\gamma = 10^6$. In fig. 1, this situation would correspond to the dark green area covering all the section of the green cone. The emission in the source frame could be beamed in a much narrower cone corresponding to $A_{\rm cone} \sim 100$. Then the burst duration would be divided by $A_{\rm cone}$, and would reach 1.3-13 ms. With a total duration of the bursts of about 5 ms, we can make the hypothesis that the contributions from τ_1 and τ_2 are similar, of a few milliseconds each.

The duration τ_2 associated with the size of the source is given by

$$\left(\frac{\tau_2}{\rm s}\right) = 240 \left(\frac{\Delta_2}{\rm deg}\right) \left(\frac{T_{orb}}{\rm day}\right). \tag{20}$$

The angle Δ_2 is actually the apparent size of the emitting region seen from the neutron star (MZ14), and T_{orb} the orbital period of the companion. Following Kepler's third law

$$\left(\frac{T_{orb}}{\rm yr}\right) = \left(\frac{M_{Sun}}{M_*}\right)^{1/2} \left(\frac{r}{\rm UA}\right)^{3/2}. \tag{21}$$

We consider a NS mass M_* =1.4 solar mass; the effective radius R_S of the source is

$$\left(\frac{R_S}{\rm m}\right) \sim 3.\,10^4 \left(\frac{\tau_2}{\rm s}\right) \left(\frac{\rm UA}{r}\right)^{1/2} \tag{22}$$

In MZ14, we estimated the angle between the Alfvén wing that emits the radio-waves and the radial direction. In the present case with $\gamma = 10^5$ to 10^6, this angle $\delta \leq 10^{-6}$ deg. At close distance to the companion, the Alfvén wing is mostly hidden behind it. We can expect that the wing is therefore not thus formed. But at a distance $l \sim R_S/\delta$, a part of thickness R_S is directly exposed to the pulsar wind (Fig. 1). Since R_S is the source radius, we can consider that the source is situated at a distance of the order of $l = R_S/\delta$ behind the companion. For $R_S \sim 100$ m, this corresponds to a distance $l \sim 5$ millions km. The time required to cover this distance at the speed of light (that is approximately the velocity of the wind) is 15 s. In the reference frame of the source, with $\gamma \sim 10^5$, this corresponds to a duration larger than 10^{-4} s, and we can expect that this is enough for the ultra-relativistic wind plasma to develop an instability causing coherent radio emissions.

These times correspond to the observation of the source when the direction of the beam is constant.

Actually, the magnetic field is not constant in the pulsar wind, and its oscillations can explain why radio emissions associated with a single asteroid cannot be seen at every

orbital period. The direction of the wind magnetic field oscillates at the spin period P_* of the pulsar which induces a slight variation of the axis of the emission cone due to relativistic aberration (see MZ14). In the reference frame of the source, the important slow oscillation (period P_*) of the magnetic field can induce stronger effects on the plasma instability, and therefore, on the direction of the emitted waves. In the observer's frame, this will consequently change the direction of emission *within* the cone of relativistic aberration. These small changes of direction combined with the long distance between the source and us will affect our possibility of observing the signal. According to the phase of the pulsar rotation, we may, or may not actually observe the source signal. In the case of a millisecond pulsar, this can change at a similar rate, and the pulse, roughly estimated in the range 1.3 to 13 ms in the above paragraph can be shortened. It is also possible, for a fast rotating pulsar, that we observe separate peaks of emission, with a time interval ~ 1 ms or more. Actually, bursts with such multiple peaks of emission (typically 2 or 3) have been observed with FRB 181222, FRB 181226, and others (CHIME/FRB Collaboration et al. 2019) and FRB 121102 (Spitler et al. 2016).

7. Parametric study

We wanted to test if medium and small solid bodies can produce FRBs. We conducted a few parametric studies based on sets of parameters compatible with neutron stars and their environment. They are based on the equations (4,5,17-19,22) presented above. We then selected the cases that met the following conditions: (1) the observed signal amplitude on Earth must exceed 1 Jy; (2) the companion must be in solid state with no melting/evaporation happening; (3) the radius of the source must exceed the maximum local Larmor radius. This last condition is a condition of validity of the MHD equations that support the theory of Alfvén wings. Practically, the larger Larmor radius might be associated with electron and positrons. In our analysis, this radius is compiled for hydrogen ions at the speed of light, so condition (3) is checked conservatively.

7.1. Medium-size and small-size companions

We first choose magnetic fields and rotation periods, relevant both to standard pulsars and to young and recycled millisecond pulsars. All combinations of the parameters listed in Table 2, resulting in 435,456 sets, were tested against the above conditions. Within the 435,456 tested sets of parameters, 7,910 filled these conditions. According to the present model, they are appropriate sets of parameters for FRB production. This is evidence of validity of the pulsar/companion model of repeating FRBs.

The parameters explored in Table 2 show that with small companions, large pulsar period $P_* \sim 1$ s cannot cause FRBs seen at 1 Gpc. Therefore, we did another study, whose parameters are summarized in Table 3. These parameters put emphasis on higher

Table 2. Parameter set of the first parametric study of FRBs produced by pulsar companions of medium and small size. The last column is the number of values tested for each parameter. The total number of calculations is the product of all values in the last column, i.e. 435,456.

Input parameters	Notation	Values	Unit	Number of val.
NS magnetic field	B_*	$10^5, 10^8$	T	2
NS radius	R_*	$10, 20$	km	2
Rotation period	P_*	$0.01, 0.1, 1$	s	3
NS temperature	T_*	$2, 5, 10$	10^5 K	3
wind Lorentz factor	γ	$10^4, 10^5, 10^6$		3
radio efficiency	ϵ	$10^{-3}, 10^{-4}$		2
NS-companion distance	r	0.01×2^n $n \in \{0, 7\}$	AU	8
companion radius	R_c	$10.^n$ $n \in \{0, 6\}$	m	7
Emission solid angle	Ω_A	$0.1, 1, 10$	sr	3
Power input	$(1-f)g\dot{E}_{\rm rp}$	$10^{23}, 10^{25}, 10^{27}, 10^{29}$	W	4
Companion conductivity	σ_c	$10^{-3}, 10^2, 10^7$	Mho	3
Distance to observer	D	1	Gpc	1
bandwidth	Δf	$\max(1, f_{ce}/10)$	GHz	1
FRB duration	τ	$5.\,10^{-3}$	s	1

Table 3. Second set of input parameters for the parametric study for pulsars, focusing on strong NS magnetic fields, short NS rotational periods and large energy inputs. The last column is the number of values tested for each parameter. Only the lines that differ from Table 2 are shown. The total number of parameter sets is the same as in Table 2.

Input parameters	Notation	Values	Unit	Number of val.
NS magnetic field	B_*	$10^7, 10^8$	T	2
Rotation period	P_*	$0.01, 0.3, 0.1$	s	3
Power input	$(1-f)g\dot{E}_{\rm rp}$	$10^{25}, 10^{27}, 10^{28}, 10^{29}$	W	4

magnetic fields and short pulsar periods, and accordingly large energy inputs. We again tested 435,456 parameter sets, out of which we got 11,158 positive results. Among them, 6,390 solutions provide bursts above 10 Jy, and 4,958 solutions provide bursts above 30 Jy, then comparable to the Lorimer burst.

The repeating known FRBs have high and irregular repetition rates. They would more probably be associated with smaller and more numerous asteroids. For instance, the disruption of a 100 km body could produce about 10^3 asteroids of size $R_c = 10$ km. So we restricted the above parametric study to asteroids of size $R_c \leq 10$ km. We also considered energy inputs $(1-f)g\dot{E}_{\rm rp} > 10^{27}$ W, because smaller values would not be realistic for short period and high magnetic field pulsars. We found 96 sets of parameters that would allow for observable FRB at 1 Gpc. The retained values correspond to $B_* = 10^8$ T, with

Table 4. Examples illustrating the results of the parametric studies in Tables 2 and 3 for pulsars with small companions. Input parameters in upper lines (above double line). We abbreviate the maximal admissible value of $(1-f)g\dot{E}_{rp}$ as E_{max}.

Parameter	B_*	R_*	P_*	T_{*maxi}	γ	ϵ	r	R_c	Ω_A	E_{max}	σ_C	f_{ceo}	S	R_S	ρ_{Li}
Unit	T	km	s	K			AU	km	rd	W	mho	Hz	Jy	km	m
Standard psr	10^8	20	0.1	5.10^5	10^6	10^{-3}	0.08	10	0.1	10^{27}	10^7	$1.6\,10^{13}$	2.04	0.6	0.005
Lorimer	10^8	20	0.01	10^6	10^6	10^{-3}	0.08	10	0.1	10^{27}	10^7	$1.6\,10^{13}$	204	0.6	0.005
Young ms psr	10^8	20	0.01	10^6	10^6	10^{-3}	0.64	10	0.1	10^{29}	10^7	$2.5\,10^{11}$	3.2	0.2	0.36

pulsar periods P_* of 10 to 100 milliseconds. Among the 96 cases, 24 provide bursts above 10 Jy, 6 above 30 Jy, and the maximum value corresponds to a 204 Jy burst.

All parameter sets require $\gamma = 10^6$. The pulsar energy outputs are typically $(1-f)g\dot{E}_{\rm rp} \leq 10^{29}$ W.

If the duration of the bursts was caused only by the source size, this size would be comprised between 0.1 and 1.1 km; this is compatible with the companion size which is of the same order (10 km). Unsurprisingly, because of the high NS magnetic field and the short distances, the local magnetic field is strong. The radiation cannot be caused by CMI type instability. The maximal ion Larmor radius is much smaller than the source size, confirming that there is no problem with MHD from which the Alfvén wing theory derives.

The companion conductivity is 10^7 in all cases, this means that the companion must be metal rich. A silicate body could not explain the observed FRB associated with small companion size. NS star temperatures of 10^6 K are possible. We did not test larger temperature, but this does not seem to be a constraining parameter.

A few examples taken among the 96 positive cases are displayed in table 4. Actually, if we consider lower energy fluxes of the order of $(1-f)g\dot{E}_{\rm rp} \sim 10^{25}$ W (not shown in Table 4) at the level of the companions, and therefore relax the minimum distance at which the companion can survive evaporation then it is possible to reach a signal of much above 100 Jy.

The 16.35 day periodicity from the repeating FRB 180916.J0158+65 (The CHIME/FRB Collaboration et al. 2020) would correspond, for a neutron star mass of 1.4 solar mass, to a swarm of asteroids at a distance $r = 0.14$ AU. This fits the range of values issued from our parametric study. The case of FRB 180916.J0158+65 will be studied in more details in a forthcoming study where emphasis will be put on dynamical aspects of clustered asteroids.

7.2. The model is compatible with the high Faraday rotation measure of FRB 121102

Michilli et al. (2018) have reported observations of 16 bursts associated with FRB 121102, at frequencies 4.1-4.9 Ghz with the Arecibo radio-telescope. All of them are fully linearly polarized. The polarization angles PA have a dependency in f^{-2} where f is the wave frequency. This is interpreted as Faraday effect. According to the theory generally used by radio-astronomers, when a linearly polarized wave propagates through a magnetized plasma of ions and electrons, its polarization angles PA in the source reference frame varies as $PA = PA_\infty + \theta = PA_\infty + RMc^2/f^2$ where PA_∞ is a reference angle at infinite frequency. The RM factor is called the rotation measure and

$$RM = 0.81 \int_D^0 B_\parallel(l) n_e(l) dl, \tag{23}$$

where $B_\parallel$ is the magnetic field in μG projected along the direction $\boldsymbol{n}$ of the wave vector, l is the distance in parsecs, and n_e is the electron number density in cm^{-3}.

Michilli et al. (2018) report very large values $RM_{obs} = (+1.027 \pm 0.001) \times 10^5$ rad m^{-2}. With the cosmological expansion redshift $RM_{src} = RM_{obs}(1+z)^2$ and $z = 0.193$, we have $RM_{src} = 1.46 \times 10^5$ rad m^{-2}. The RM_{obs} are so large that they could not be detected at lower frequencies, 1.1-2.4 GHz, because of depolarization in the relatively coarse bandwidths of the detectors. Measurements done later at the Green Bank Telescope at 4-8 GHz provided similar values: $RM_{src} = 1.33 \times 10^5$ rad m^{-2} (Gajjar et al. 2018).

Let us first mention that a pair-plasma does not produces rotation measure. Therefore, these RM are produced in an ion-electron plasma, supposed to be present well beyond the distances r of the pulsar companions of our model. Michilli et al. (2018) propose that the rotation measure would come from a 1 pc HII region of density $n_e \sim 10^2$ cm^{-3}. This would correspond to an average magnetic field $B_\parallel \sim 1$ mG. But for comparison, average magnetic fields in similar regions in our Galaxy correspond typically to 0.005 mG. Therefore. It is suggested that the source is in the vicinity of a neutron star and, more plausibly, of a magnetar or a black hole.

We have made a parametric study of our model where the NS is a magnetar. The parameters are summarized in Table 5. Because the thermal radiation of magnetar NS can exceed those of pulsar NS by a factor 10^3 (Enoto et al. 2019), we considered magnetar temperatures up to 6.10^6 K. Over the 248,832 tested sets of parameters, 2,182 fit the conditions defined in section 7, and 1,062 are associated with bursts above 30 Jy.

Because FRB121102 is repeating, we suspect numerous small bodies. So we analyzed a subset of the previous parametric study, setting a companion radius $R_c \leq 10$ km, and parameters fitting an idealized "standard" magnetar: $B_* = 10^{12}$ T and $(1-f)g\dot{E}_{\rm rp} = 10^{28}$ W. Then, we got 202 sets of parameters satisfying the requirements defined in section 7. A few examples are displayed in table 6. Actually, they provide particularly energetic signals, up to $\sim 10^5$ Jy is displayed in the first line. Therefore, one can relax a few

Table 5. Sets of input parameters for the parametric study for magnetars. Only the lines that differ from Table 2 are plotted.

Input parameters	Notation	Values	Unit	Number of val.
NS magnetic field	B_*	$10^{10}, 10^{12}$	T	2
NS radius	R_*	12	km	1
Rotation period	P_*	$0.1, 1, 3, 10$	s	4
NS temperature	T_*	$1.5, 3, 6$	10^6 K	3
companion radius	R_c	$10.^n$ $n \in \{0, 5\}$	m	6
Power input	$(1-f)g\dot{E}_{\rm rp}$	$10^{27}, 10^{28}, 10^{29}, 10^{30}$	W	4

Table 6. Sets of parameters for FRB associated with magnetars and small companions. Input parameters in upper lines (above double line). Output values below double line.

Parameter	B_*	R_*	P_*	T_{*maxi}	γ	ϵ	r	R_c	Ω_A	E_{max}	σ_C	f_{ceo}	S	R_S	ρ_{Li}
Unit	T	km	s	K			AU	km	rd	W	mho	Hz	Jy	km	m
Super-FRB	10^{12}	12	0.1	3.10^6	10^6	10^{-3}	1.28	10	0.1	10^{28}	10^7	$2.2\,10^{14}$	10^5	0.15	4.10^{-4}
slower wind	10^{12}	12	3	3.10^6	10^5	10^{-4}	0.32	10	0.1	10^{28}	10^7	$3.5\,10^{14}$	1.8	0.29	2.510^{-4}
small R_c	10^{12}	12	1	6.10^6	10^6	10^{-4}	1.28	1	0.1	10^{28}	10^7	$2.2\,10^{14}$	1.0	0.15	4.10^{-4}

parameters. This is done in the second line where a set of parameters providing a 1-2 Jy signal, compatible with FRB121102, is given. A companion radius of 10 km, a wind Lorentz factor $\gamma = 10^5$, and a radio efficiency $\epsilon = 10^{-4}$ is proposed. The same signal can also be given with a $R_c = 1$ km companion, and $\gamma = 10^6$. The third line shows a signal of 1 Jy associated with companions size $R_c = 1$ km only, in spite of a distance r =1.28 AU and a low radio yield $\epsilon = 10^{-4}$. This case allows for a hotter NS, with a temperature $T_* = 6.10^6$ K. Nevertheless, there are some limitations of the parameters. For instance, among these 202 explored solutions for small bodies $R_c < 10$ km, none correspond to a magnetar period $P_* = 10$s.

8. Discussion

Mottez and Zarka (MZ14) showed that planets orbiting a pulsar in interaction with the wind could cause FRBs. Their model predicts that FRBs should repeat periodically with the same period as the orbital period of the planet. An example of possible parameters given in Mottez & Zarka (2014) was a planet with a size $\sim 10^4$ km at 0.1 AU from a recycled millisecond neutron star. Later, Chatterjee et al. (2017) published the discovery of the repeating FRB121102. The cosmological distance of the source (1.7 Gpc) was confirmed. But the repeater FRB121102, as well as the others discovered since then, are not periodic.

In the present paper, we consider that irregular repeating FRBs can be triggered by swarms of small bodies orbiting in an asteroid belt surrounding a pulsar. After adding

some thermal considerations that were not included in MZ14, we conducted several parametric studies that showed that repeating FRBs as well as non-repeating ones can be generated by small bodies in the vicinity of a pulsar (a young one rather than a recycled millisecond pulsar) or a magnetar. Some parameters sets even show that 10 km bodies at a close distance from a magnetar could survive evaporation and emit FRBs that could be seen at a distance of 1 Gpc with a flux of about 100 kJy !

In MZ14, it was supposed that the radio waves would be emitted by the cyclotron maser instability (CMI). But the frequency of CMI is slightly above the electron gyrofrequency, that, with the retained parameters, is not in the radio-frequencies range. Therefore, another emission mechanism must be sought. We know that it is possible to generate strong coherent emissions at a frequency much below the electron gyrofrequency. For instance, this is what happens with pulsar coherent radio emissions, as is also expected with FRB. Of course, the wind magnetic field near the companions is not comparable to those in the pulsar inner magnetosphere, and we probably cannot explain radio waves in the wind crossing the Alfvén wing behind a pulsar companion like we would explain those generated near the neutron star. But if the magnetic field near the companion is smaller than near the star, the plasma frequency is also much lower, and maybe their ratio is not so different.

Whatever the radio emission process, our parametric study is based on the hypothesis that in the source reference frame, the wave directions spread over a solid angle $\Omega_A \sim 0.1$, corresponding to the parameter $A \sim 100$. Actually, this may not be the right value, and we could upgrade the parametric study when we have better constrains. But it seems that a process causing isotropic radio emissions (in the source frame) would produce longer bursts, in the range 0.1-1 second instead of a few milliseconds.

Other models invoke asteroids orbiting a pulsar as possible sources of FRBs (Geng & Huang 2015; Dai et al. 2016). In Dai et al. (2016), the authors consider the free fall of an asteroid belt into a highly magnetized pulsar, which is compatible with the repetition rate of FRB121102. The asteroid belt is supposed to be captured by the neutron star from another star (see Bagchi (2017) for other capture scenarios). The main energy source is the gravitational energy release related to tidal effects when the asteroid passes through the pulsar breakup radius. After Colgate & Petschek (1981), and with their fiducial values, they estimate this power to $\dot{E}_G \sim 1.2\,10^{34}$ W. Even if this power is radiated isotropically from a source at a cosmological distance, this is enough to explain the observed FRB flux densities. Dai et al. (2016) developed a model to explain how a large fraction of this energy is radiated in the form of radio waves. As in Mottez & Zarka (2014), they involve the unipolar inductor, with an electric field mostly in the form $\boldsymbol{E}_2 = -\boldsymbol{v}_{ff} \times \boldsymbol{B}$. (We note E_2 as in Dai et al. (2016).) Then, the authors argue that this electric field can accelerate electrons up to a Lorentz factor $\gamma \sim 100$, with a density computed in a way similar to the Goldreich-Julian density in a pulsar magnetosphere. These accelerated electron

would cause coherent curvature radiation at frequencies of the order of ~ 1 GHz. Their estimate of the power associated with these radio waves would be $\dot{E}_{radio} \sim 2.6 \times 10^{33}$ W $\sim 0.2\dot{E}_G$. This process might be also applicable to our model.

Nevertheless, besides the positive aspects of the model developed in Dai et al. (2016), we notice that it predicts high efficiency of the radio emission ($\epsilon \sim 10^{-2}$ at best), when our estimates are in the range $\epsilon \sim 10^{-3}$ or less. Actually, we must notice that the asteroid does not fall into a vacuum as is implicitly supposed in Dai et al. (2016). It falls across the plasma expelled by the pulsar. We cannot neglect this fact. Because of this plasma, the unipolar inductor does not develop an accelerating field E_2 given in their paper. Indeed, the electric field is partially screened by the pulsar plasma, and the plasma reacts to this screening with the development of an Alfvén wing. Historically, we can notice that the Alfvén wing model was elaborated in Neubauer (1980) in the context of the Io-Jupiter interaction, precisely because the simple unipolar inductor theorized by Goldreich & Lynden-Bell (1969b) did not explain the in-situ observations by the pioneer NASA spacecraft. As we have seen, the Alfvén wing is carried by a strong electric current, but the velocity and the density of the particles that carry it cannot be computed as in Dai et al. (2016), and we strongly suspect that the total energy radiated in the form of radio waves is one order of magnitude below their estimate (that would correspond to our supposed efficiency $\epsilon \sim 10^{-3}$).

In the consideration of the thermal constraints, we have treated separately the Alfvén wing and heating by the Poynting flux of the pulsar wave. For the latter, we have used the Mie theory of diffusion which takes into account the variability of the electromagnetic environment of the companion, but neglects the role of the plasma surrounding it. On the other hand, the Alfvén wing theory, in its present state, takes the plasma into account, but neglects the variability of the electromagnetic environment. A unified theory of an Alfvén wing in a varying plasma would allow a much better description of interaction of the companion and its environment. This subject actually goes beyond the scope of the present paper.

An important and often asked question related to the present model is the probability of occurrence of FRBs. This probability depends on the number of neutron stars in a galaxy, on the number of galaxies within a 1 or 2 Gpc range, but also on the chances of being in the line of sight of a neutron star and an asteroid orbiting it. It is also important to explain why the repetition rate of the FRB is not related to a random Poisson process. These questions are related to the orbital properties of swarms of asteroids near a neutron star. These questions invoke gravitation, tidal effects, and electrodynamics of Alfvén wings (Mottez & Heyvaerts 2011a). We plan to address these questions in a forthcoming paper.

Acknowledgement

G. Voisin acknowledges support of the European Research Council, under the European Unions Horizon 2020 research and innovation programme (grant agreement No. 715051; Spiders).

References

Abdo, A. A., Ackermann, M., Ajello, M., et al. 2010a, ApJ, 713, 154

Abdo, A. A., Ackermann, M., Ajello, M., et al. 2010b, ApJ, 708, 1254

Abdo, A. A., Ajello, M., Allafort, A., et al. 2013, The Astrophysical Journal Supplement, 208, 17

Bagchi, M. 2017, ApJ, 838, L16

Becker, W. 2009, in Astrophysics and Space Science Library, Vol. 357, Astrophysics and Space Science Library, ed. W. Becker, 133–136

Cerutti, B. & Philippov, A. A. 2017, A&A, 607, A134

Chatterjee, S., Law, C. J., Wharton, R. S., et al. 2017, Nature, 541, 58

CHIME/FRB Collaboration, Andersen, B. C., Bandura, K., et al. 2019, ApJ, 885, L24

Colgate, S. A. & Petschek, A. G. 1981, ApJ, 248, 771

Cordes, J. M., Wasserman, I., Hessels, J. W. T., et al. 2017, The Astrophysical Journal, 842, 35

Dai, Z. G., Wang, J. S., Wu, X. F., & Huang, Y. F. 2016, ApJ, 829, 27

Enoto, T., Kisaka, S., & Shibata, S. 2019, Reports on Progress in Physics, 82, 106901

Freund, H. P., Wong, H. K., Wu, C. S., & Xu, M. J. 1983, Physics of Fluids, 26, 2263

Gajjar, V., Siemion, A. P. V., Price, D. C., et al. 2018, ApJ, 863, 2

Geng, J. J. & Huang, Y. F. 2015, ApJ, 809, 24

Ghisellini, G. 2017, MNRAS, 465, L30

Gillon, M., Triaud, A. H. M. J., Demory, B.-O., et al. 2017, Nature, 542, 456

Goldreich, P. & Lynden-Bell, D. 1969a, Astrophysical Journal, 156, 59

Goldreich, P. & Lynden-Bell, D. 1969b, ApJ, 156, 59

Gurnett, D. A., Averkamp, T. F., Schippers, P., et al. 2011, Geophys. Res. Lett., 38, L06102

Hess, S., Zarka, P., & Mottez, F. 2007, Planet. Space Sci., 55, 89

Jewitt, D. C., Sheppard, S., & Porco, C. 2004, Jupiter's outer satellites and Trojans, 263–280

Jewitt, D. C., Trujillo, C. A., & Luu, J. X. 2000, AJ, 120, 1140

Karuppusamy, R., Stappers, B. W., & van Straten, W. 2010, Astronomy and Astrophysics, 515, A36

Katz, J. I. 2017, MNRAS, 467, L96

Kirk, J. G., Skjæraasen, O., & Gallant, Y. A. 2002, A&A, 388, L29

Kotera, K., Mottez, F., Voisin, G., & Heyvaerts, J. 2016, A&A, 592, A52

Lentz, W. J. 1976, Applied Optics, 15, 668

Louis, C. K., Lamy, L., Zarka, P., Cecconi, B., & Hess, S. L. G. 2017, Journal of Geophysical Research (Space Physics), 122, 9228

Melrose, D. B. & Rafat, M. Z. 2017, 932, 012011

Michilli, D., Seymour, A., Hessels, J. W. T., et al. 2018, Nature, 553, 182

Mottez, F. & Heyvaerts, J. 2011a, Astronomy and Astrophysics, 532, A22+

Mottez, F. & Heyvaerts, J. 2011b, Astronomy and Astrophysics, 532, A21+

Mottez, F. & Zarka, P. 2014, Astronomy and Astrophysics, 569, A86

Neubauer, F. M. 1980, Journal of Geophysical Research (Space Physics), 85, 1171

Ng, C. W., Takata, J., Strader, J., Li, K. L., & Cheng, K. S. 2018, ApJ, 867, 90

Oostrum, L. C., Maan, Y., van Leeuwen, J., et al. 2019, arXiv e-prints, arXiv:1912.12217

Pétri, J. 2016, Journal of Plasma Physics, 82, 635820502

Petroff, E., Barr, E. D., Jameson, A., et al. 2016, PASA, 33, e045

Pryor, W. R., Rymer, A. M., Mitchell, D. G., et al. 2011, Nature, 472, 331

Saur, J., Neubauer, F. M., Connerney, J. E. P., Zarka, P., & Kivelson, M. G. 2004, 1, 537

Scholz, P., Spitler, L. G., Hessels, J. W. T., et al. 2016, ApJ, 833, 177

Shannon, R. M., Cordes, J. M., Metcalfe, T. S., et al. 2013, The Astrophysical Journal, 766, 5

Shannon, R. M., Osłowski, S., Dai, S., et al. 2014, Monthly Notices of the Royal Astronomical Society, 443, 1463

Spitler, L. G., Scholz, P., Hessels, J. W. T., et al. 2016, Nature, 531, 202

The CHIME/FRB Collaboration, Amiri, M., Andersen, B. C., et al. 2020, arXiv e-prints, arXiv:2001.10275

Timokhin, A. N. & Arons, J. 2013, MNRAS, 429, 20

Wilson, D. B. & Rees, M. J. 1978, MNRAS, 185, 297

Wolszczan, A. & Frail, D. A. 1992, Nature, 355, 145

Zarka, P., Marques, M. S., Louis, C., et al. 2018, A&A, 618, A84

Zavlin, V. E. 2009, in Astrophysics and Space Science Library, Vol. 357, Astrophysics and Space Science Library, ed. W. Becker, 181